

Chapter 3

Fluoride sensing study of amine and nitro substituted thiourea derivatives in aqueous medium

3.1. Introduction

Over the past five decades, significant progress has been made in anion recognition, driven by the fundamental importance of anions in chemical, environmental, and biological processes [1-3]. A diverse array of synthetic receptors has been developed, with urea- and thiourea-based molecules gaining particular attention. These molecules, offering directional binding sites, are attractive anion receptors due to their ability to bind anions like fluoride and acetate primarily through hydrogen-bonding interactions under neutral conditions [4-7]. The two imine ($-NH$) groups on each urea or thiourea functionality provide excellent binding potential as well as directionality, mimicking natural processes in living cells. Additionally, the thiocarbonyl groups ($C=S$) in a thiourea-functionalized receptor enhances acidity, potentially reinforcing its anion recognition affinity compared to an analogous urea-based receptor having a carbonyl ($C=O$) group. This unique interaction profile gives thiourea-based sensors distinct selectivity and enhanced binding affinity compared to urea-based sensors. The increased acidity of the thiocarbonyl groups ($C=S$) in thiourea-functionalized receptors further enhances anion binding ability compared to analogous urea-based receptors with carbonyl groups ($C=O$) and their versatile chemical structures allow for easy modifications to tailor sensor properties for various applications, enhancing solubility, stability, and detection capabilities in different environments [7,8]. Urea and thiourea compounds are simple and cost-effective to synthesize, making them widely accessible, however, they face challenges in selectively sensing fluoride over acetate and dihydrogen phosphate in non-aqueous media. Typically, fluoride detection by thiourea molecules is driven predominantly by its basicity, whereas acetate sensing is facilitated by binding site complementarity with the two $-NH$ groups. Interestingly, sulphur forms weaker hydrogen bonds than oxygen. This characteristic makes aligning the thiourea functionality for complex formation with fluoride ions much easier compared to urea. Thiourea's N-H acidity is high relative to urea, therefore they are more prone for deprotonation upon interaction with F^- . Furthermore, beyond anion sensing, thiourea-based molecules have been extensively studied as ligands for complexation with transition metal ions such as Cu (II), Ni (II), Zn(II), Co(II), Fe(III), etc.

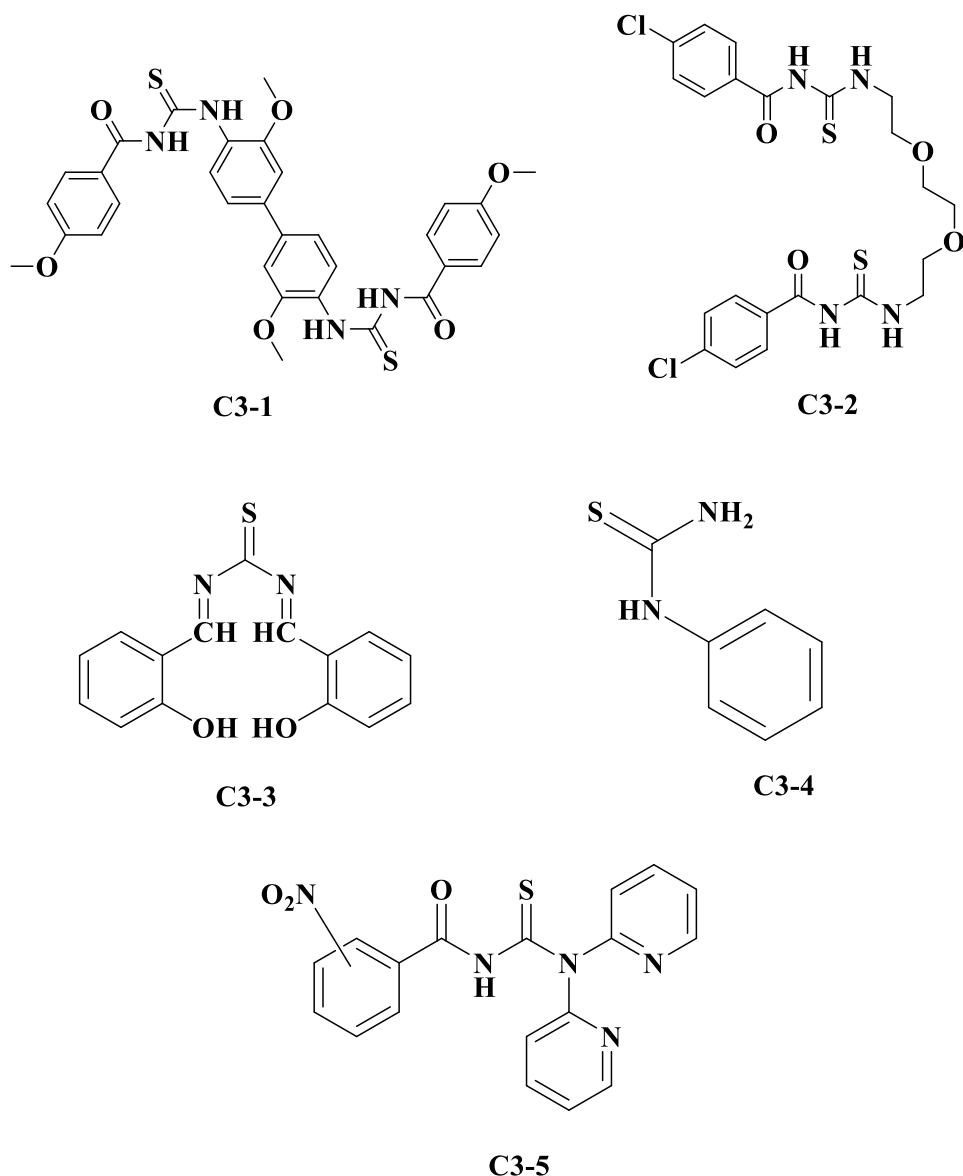


Figure 3.1: Literature report of some thiourea based molecules for metal ion sensing [9-13].

Earlier reports revealed that in the presence of anions, either anion-NH hydrogen bonding or anion-induced deprotonation of the -NH group is involved, leading to fluorescence quenching by the photo-induced electron transfer (PET) mechanism or a red shift in absorption due to the charge transfer (CT) mechanism. Fabbrizzi *et al.* have reported that the deprotonation propensity could be enhanced by increasing the acidity of the hydrogen bond donor and the basicity of the anions [14,15]. Based on this hypothesis, Li and co-workers synthesized a benzimidazole-isoquinolinone incorporated thiourea-based fluoride ion sensor [16].

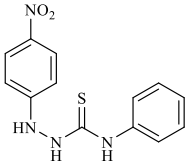
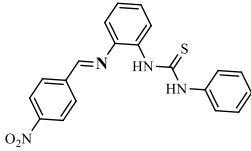
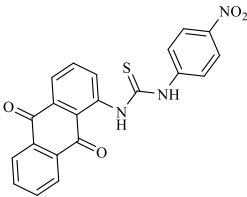
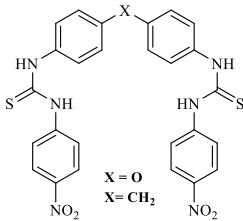
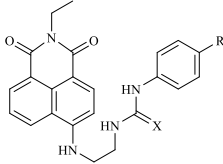
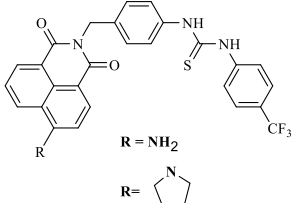
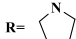
Probe	Fluoride salt used	Solvent of study	Types of Sensors	References
	TBAF as F ⁻ ion source	DMSO	Chromogenic	[19]
	TBAF as F ⁻ ion source	CH ₃ CN	Chromogenic	[20]
	TBAF as F ⁻ ion source	CH ₃ CN	Chromogenic	[21]
 X = O X = CH ₂	TBAF as F ⁻ ion source	DMSO	Chromogenic	[22]
 X = S; R = H X = S; R = CF ₃ X = O; R = CF ₃	TBAF as F ⁻ ion source	DMSO	Chromogenic	[23]
 R = NH ₂ R = 	TBAF as F ⁻ ion source	DMSO	Chromogenic	[24]

Table 3.1: Literature report of some thiourea based molecules for anion ion sensing.

and demonstrated a colorimetric change due to the deprotonation of the acidic proton in the thiourea moiety by the fluoride ion. Although the detection limit is in the nanomolar range, all sensing was performed in an organic medium using tetrabutylammonium fluoride as the analyte.

Additionally, numerous reports involve anion recognition in the presence of metal ions by (thio)urea ligands that possess both metal and anion binding sites. These reports highlight key prospects, such as the coordination of a metal cation enhancing the hydrogen bond donor tendencies of the (thio)urea moiety and creating a preorganized anion binding environment with higher selectivity for a specific anion. For example, Carreira-Barral and co-workers reported a receptor containing both cation and anion binding sites in the form of a di(2-picoly)amine (dpa) and urea unit, respectively [17]. Their work demonstrated that metal (Cu^{2+} and Zn^{2+}) coordination enhances the deprotonation ability of urea NHs in DMSO solution with basic anions like fluoride and acetate. Following such observations, Das *et al.* reported a receptor with a hydroxyl moiety near the thiourea binding units, which has a comparatively lower pKa value than the thiourea NHs [18]. The deprotonation of the acidic proton by the fluoride ion is accompanied by the in-situ Ni(II) metal complexation favouring the deprotonation reaction between the thiourea and fluoride. The study conveyed that the introduction of metal stabilizes the conjugate base of the receptor, increasing the sensitivity and selectivity toward the sensing of aqueous fluoride. Like Das and co-workers, herein we have investigated the effect of supplementary $-\text{NH}_2$ group in the transition metal mediated strategy in reinforcing the fluoride recognition affinity of the receptor in aqueous medium (Figure 3.2). The $-\text{NH}_2$ group introduced in the phenyl moiety is presumed to facilitated both fluoride as well as metal coordination. Furthermore, we introduced the $-\text{NO}_2$ groups in the aniline subunit of the thiourea with a believe that it will enhance the colorimetric responds due to the inbuild charge transfer chromophore, *i.e.* nitro aniline.

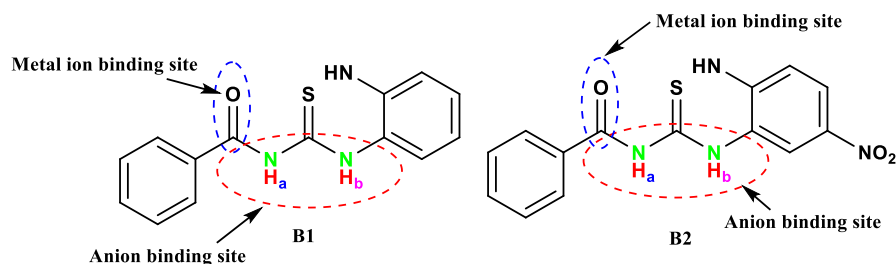


Figure 3.2: Structure of probe molecules **B1** & **B2**.

3.2. Objective of the study

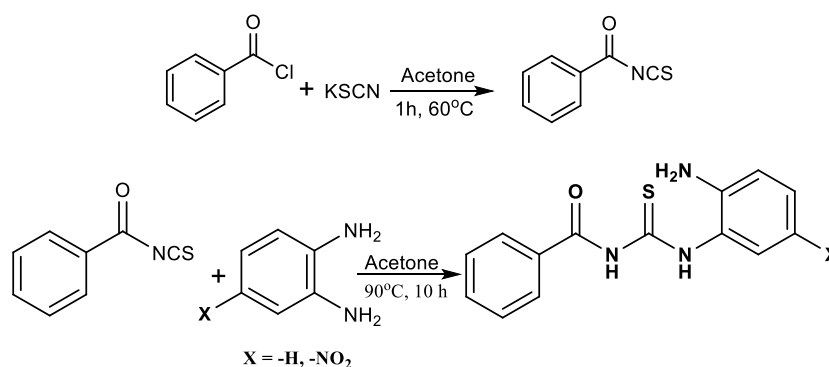
The objective of the study reported in this chapter are:

- Demonstration of the fluoride sensing affinity of the thiourea based receptor (**B1** & **B2**) in aqueous medium by following the metal mediated strategy based on hypothesis 1.
- Validation of the strategy with UV-Vis spectroscopy and electrochemical techniques like cyclic voltammogram and differential pulse voltammetry.
- Study of the efficiency of the methodology with some real-life samples.

3.3. Results and discussion

3.3.1 Synthesis and Characterization

The synthesis of the receptors was performed by following scheme 3.1 and characterized by standard spectroscopic techniques.



Scheme 3.1: Synthesis of the receptor **B1** (X=H) and **B2**(X= -NO₂).

0.925 mmol of Potassium thiocyanate was dissolved in 15 mL acetone. To it, 0.925 mmol of the Benzoyl chloride was added dropwise with constant stirring. The mixture was then refluxed at 55° - 60° C for 1 h and subsequently the reaction was kept to reach room temperature. The reaction mixture was filtered and to the filtrate, 0.925 mmol of *o*-Phenylene diamine in acetone solution was added dropwise with constant stirring. The mixture was then refluxed at 90° C for 10 h and thereafter the solution was concentrated by removing the acetone till dark brown liquid compound was obtained. To the concentrated solution ice cold water was poured and the mixture was agitated vigorously till the compound solidified. The mixture filtered out and the precipitate was washed vigorously with cold ethanol.

B1: Appearance: Pale Brownish red, Yield: 60 %, FTIR (cm^{-1}): $\nu(\text{NH}) = 3300$, $\nu(\text{C—N}) = 1700$ and $\nu(\text{C-N}) = 1345$. ^1H NMR (400 MHz, DMSO) δ 12.01 (s, 1H), 11.56 (s, 1H), 8.07 – 8.03 (m, 3H), 7.76 – 7.70 (m, 1H), 7.60 (m, $J = 8.4, 7.1$ Hz, 3H), 7.37 (m, $J = 7.9, 1.5$ Hz, 1H), 7.08 (m, $J = 8.1, 7.3, 1.6$ Hz, 1H), 6.84 (m, $J = 8.0, 1.4$ Hz, 1H), 6.66 (m, $J = 7.5, 1.4$ Hz, 1H), 5.16 (s, 2H). ^{13}C NMR (101 MHz, DMSO) δ 180.76, 168.63, 143.81, 133.45, 132.87, 129.13, 128.88, 128.20, 127.90, 123.64, 116.27

B2: Appearance: Dark yellow powder, Yield: 90 %, FTIR (cm^{-1}): $\nu(\text{NH}) = 3319$, $\nu(\text{C—N}) = 1665$, $\nu(\text{N—O}) = 1578$ and $\nu(\text{C-N}) = 1301$. ^1H NMR (400 MHz, DMSO) δ 11.91 (s, 1H), 11.68 (s, 1H), 8.10 (d, $J = 2.6$ Hz, 1H), 7.99 (m, $J = 16.2, 8.7, 2.0$ Hz, 3H), 7.70 – 7.65 (m, 1H), 7.56 (m, $J = 7.6$ Hz, 2H), 6.81 (d, $J = 9.1$ Hz, 1H), 6.75 (s, 2H). ^{13}C NMR (101 MHz, DMSO) δ 182.24, 168.62, 151.62, 135.72, 133.53, 132.82, 129.04 (d, $J = 26.2$ Hz), 126.07, 125.29, 122.06, 114.45.

We have also attempted to get the single crystals for both the receptors, however able to get good quality single crystal only for **B1** upon slow evaporation from ethanol (Appendix A.2.2, table A 2.1). The crystal structure analysis of **B1** revealed the involvement of intramolecular -NHO hydrogen bonding between the thiourea -NH and the benzoyl carbonyl moiety. It is also observed that the remaining -NH thiourea moiety involved in the intermolecular N-H...N hydrogen bonding with the anchoring -NH₂ moiety facilitating the 3D packing. Furthermore, it is observed that the thiourea S remains ideal in the solid-state supramolecular arrangement (Figure 3.3).

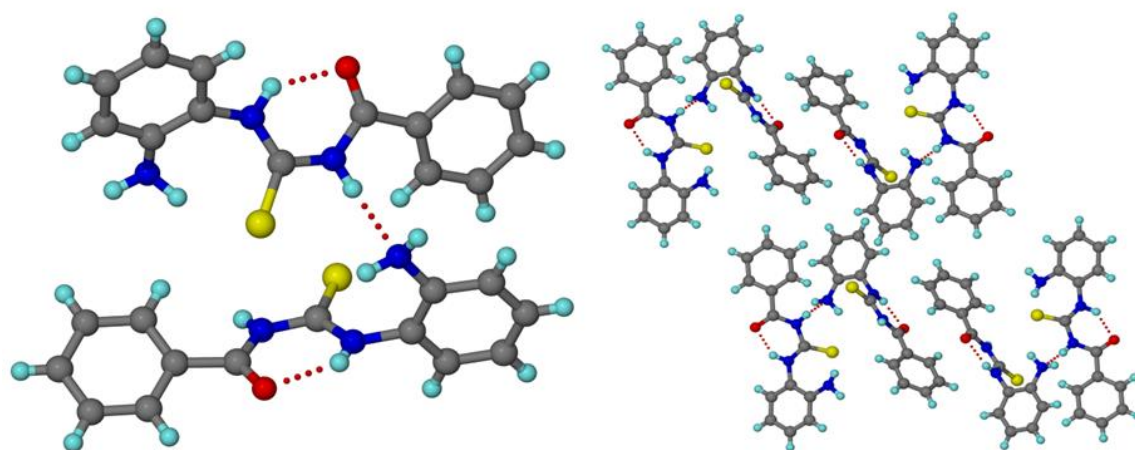


Figure 3.3: Packing diagram of **B1**.

3.3.2. Anion binding studies in DMSO medium

The anion binding affinity of probe molecules **B1** and **B2** was initially analysed using UV-Vis spectroscopy in DMSO solution. Tetrabutylammonium salt solutions of various anions (F^- , Cl^- , Br^- , I^- , ClO_4^- , HSO_4^- , $H_2PO_4^-$, AcO^- , each of 5×10^{-2} M) in DMSO were added to **B1** and **B2** solutions (6×10^{-5} M in DMSO), and the resultant colorimetric changes were monitored. The colour of **B1** in DMSO changed from colourless to yellow upon addition of F^- ion which led to the appearance of a broad peak at 320 nm in the UV-Vis spectra. UV-Vis spectra of **B2** in DMSO showed a sharp peak at 375 nm. However, addition of F^- , CH_3COO^- and $H_2PO_4^-$ to **B2** solution exhibited a noticeable colour shift from orange to blood red. The UV-Vis spectra of the **B2** solution in DMSO showed lowering of the peak intensity of the 375 nm peak with concomitant immergence of a new broad peak from 440-510 nm upon addition of the above three ions (Figure 3.4). No appreciable colour change was observed when Cl^- , Br^- , I^- , ClO_4^- , HSO_4^- were added to the **B1** and **B2** solutions in DMSO.

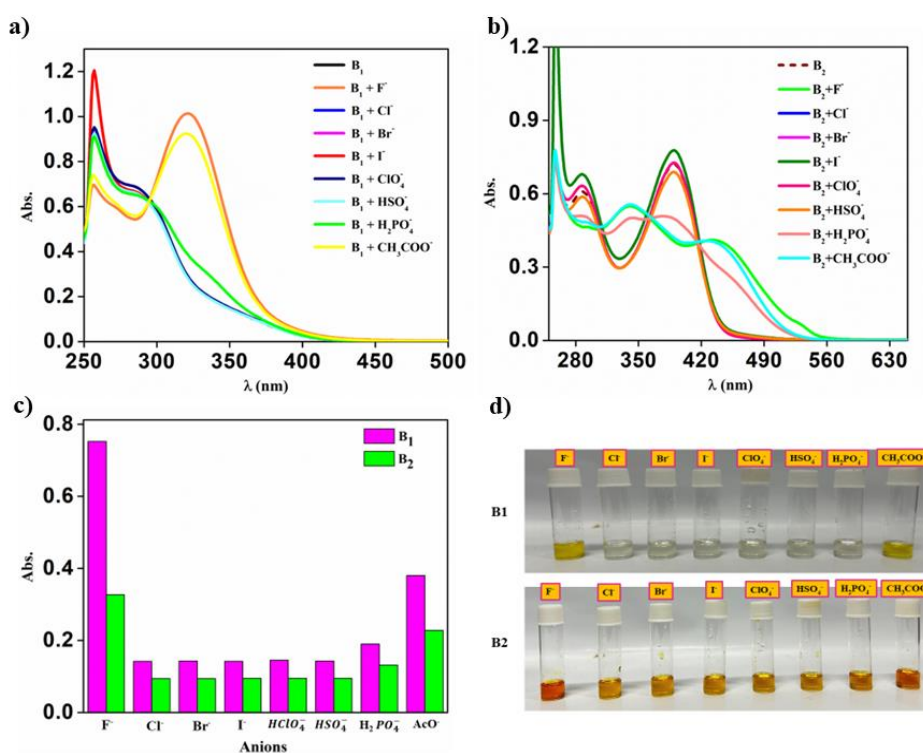


Figure 3.4: (a) UV-Vis spectra of **B1** in DMSO (6×10^{-5} M) upon addition of anions in DMSO; (b) UV-Vis spectra of **B2** in DMSO (6×10^{-5} M) upon addition of anions in DMSO; (c) Bar diagram showing changes in the absorbance of **B1** (Pink) and **B2** (Green) in DMSO (both 6×10^{-5} M concentration) upon addition of different anion solutions (5×10^{-2} M); (d) Colorimetric changes upon addition of anions to **B1** and **B2**.

This observation revealed that both compounds can selectively recognize fluoride and acetate ions in DMSO, with **B2** showing minor interference from phosphate ions (Figure 3.4). This anion screening study inferred that the introduction of -NO₂ group might enhance the acidity of the -NH proton and hence decrease the anion selectivity of receptor **B2**.

To better understand the recognition, the UV–Vis titration experiment was conducted. For **B1**, the intensity of the maximum absorption peak at 320 nm gradually augmented as the fluoride concentration increased. Similarly, the solution of **B2** showed a decrease in the intensity of the peak at 400 nm, with a concomitant evolution of the peak at 450 nm upon sequential addition of fluoride, maintaining two isosbestic points at 360 nm and 420 nm. Job's plot showed a plateau at 0.5 for **B1** and 0.43 for **B2**, confirming a 1:1 stoichiometry for the interaction with fluoride (Figure 3.5, c-d). The changes in the absorption spectra and the colorimetric response were more prominent in **B2** due to the higher acidity of the N–H hydrogen of **B2** compared to **B1**. The presence of a -NO₂ group in **B2** withdraws electron density from the N–H moiety, enhancing acidity and hence deprotonation affinity. The equilibrium constants for the interaction of **B1** and **B2** with fluoride were calculated from the titration data using Connor's equation and the Benesi-Hildebrand method (Appendix A1). Curve fitting was performed by considering absorption at wavelengths of 320 nm for **B1** and 450 nm for **B2**. A linear relationship between $(1/A - A_0)$ and the concentration of $1/[F^-]$ ($R^2 = 0.995$ for **B1** and $R^2 = 0.957$ for **B2**) was observed, yielding association constants of $4.7 \times 10^2 \text{ M}^{-1}$ for **B1** and $2.4 \times 10^4 \text{ M}^{-1}$ for **B2** (Figure 3.6, a-b). The larger equilibrium constant for **B2** is attributed to the higher acidity of the thiourea NHs. The UV–Visible experiments indicated that probes **B1** and **B2** have promising affinity for fluoride salt with an organic counter ion in DMSO.

To study the efficiency of the receptors F⁻ sensing tendency in aqueous medium we have added water to the coloured solution of the receptor molecule-F⁻ mixture (**B1**.F⁻ and **B2**.F⁻) in DMSO. It is observed that the colour immediately disappears and the intensity of the representing receptor F⁻ interaction decreases immediately upon addition of 5% V/V of water in the mixture (Figure 3.6). Furthermore, addition of aqueous solution of TBAF and NaF did not lead to any characteristic colorimetric change as observed in case of addition of TBAF in DMSO solution. This observation inferred the incapability of both the probe molecules *i.e.* **B1** and **B2** to detect F⁻ ion in water medium.

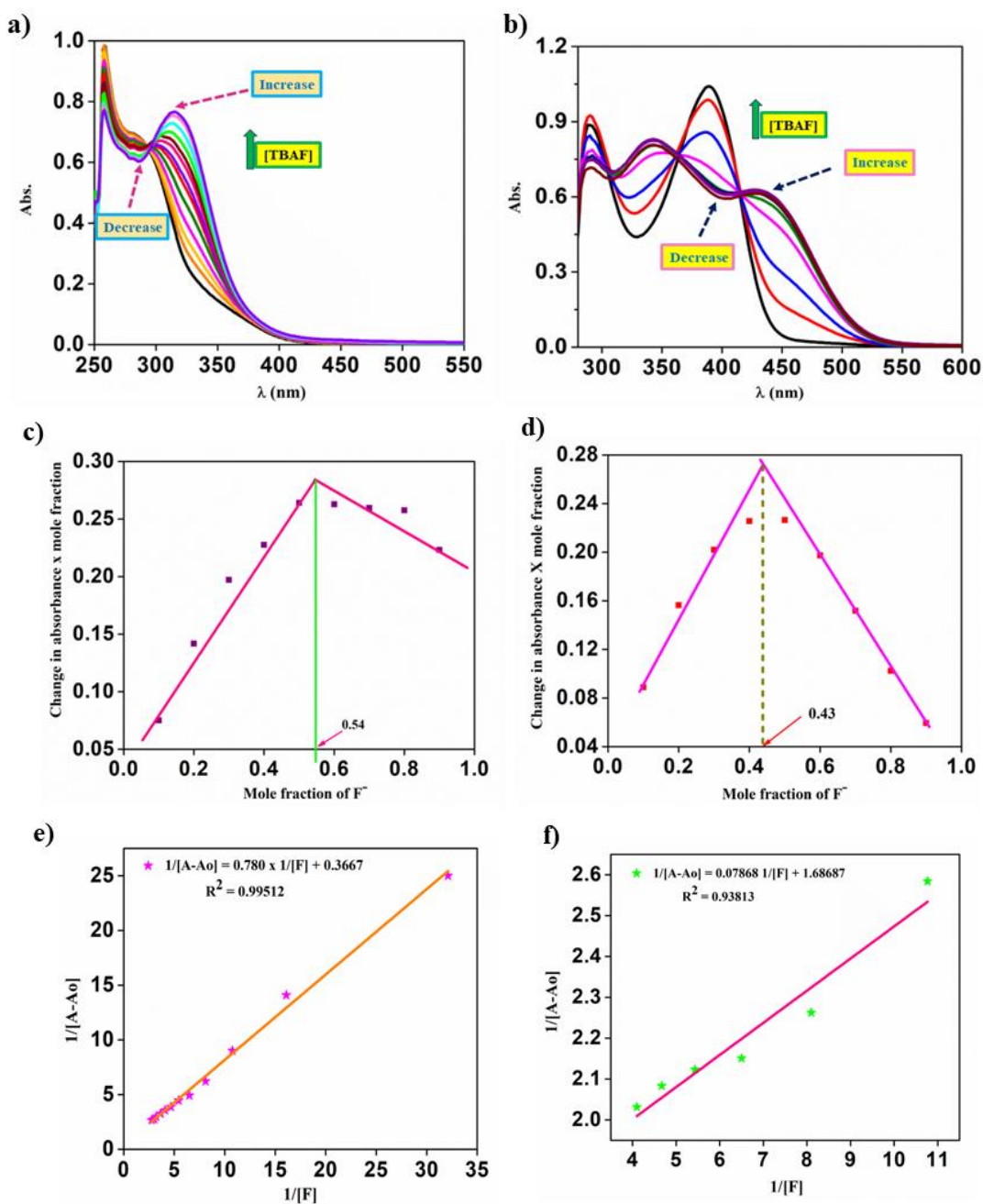


Figure 3.5: (a) UV-Vis spectra of **B1** in DMSO (6×10^{-5} M) upon gradual addition of TBAF solution in DMSO; (b) UV-Vis spectra of **B2** in DMSO (6×10^{-5} M) upon gradual addition of TBAF solution in DMSO; (c) Job's plot of **B1** representing 1:1 stoichiometric interaction between **B1** and F^- ; (d) Job's plot of **B2** representing 1:1 stoichiometric interaction between **B2** and F^- ; (e) Benesi-Hildebrand plot of **B1**-TBAF titration; (f) Benesi-Hildebrand plot of **B2**-TBAF titration.

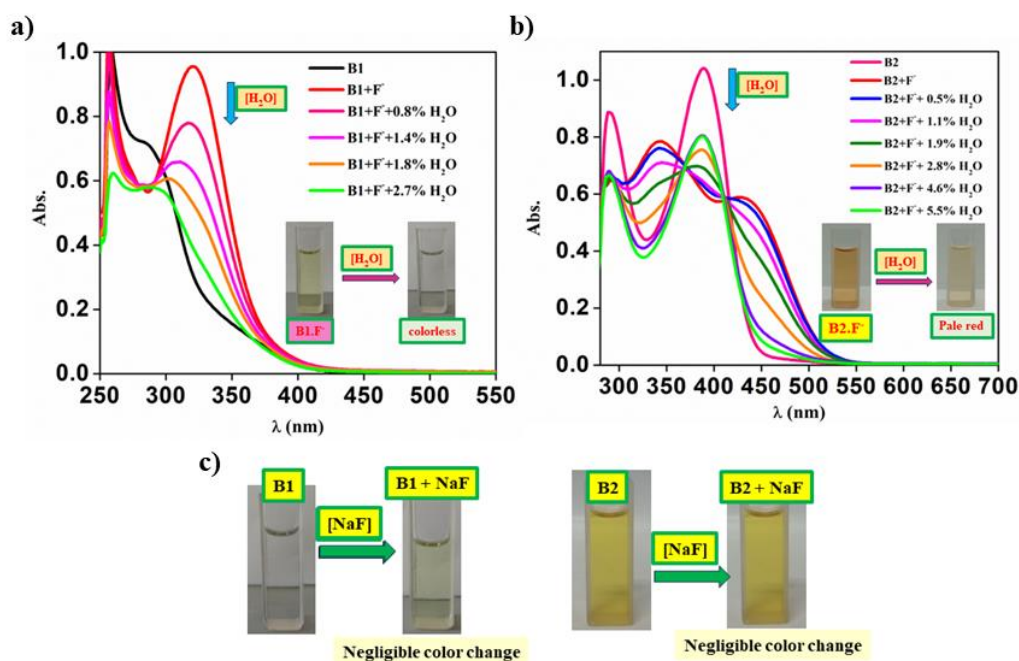


Figure 3.6: Change in UV-Vis spectra of receptor fluoride solution in DMSO upon addition of water, (a) **B1**; (b) **B2**; (c) Colorimetric change upon addition of NaF (aq) to **B1** and **B2** in DMSO.

3.3.3. $^1\text{H-NMR}$ titration study

Intrigued by observations of UV-Vis study, we conducted a $^1\text{H-NMR}$ titration experiment to further elucidate the binding mechanism between the probe molecules and F^- ions in DMSO medium. The $^1\text{H NMR}$ spectra in $\text{DMSO-}d_6$ (23×10^{-3} M) solution showed the signal for thiourea -NH protons at $\delta=11.8$ ppm and $\delta=11.5$ ppm for **B1**, and $\delta=11.8$ ppm and $\delta=12.0$ ppm for **B2**, corresponding to the -NH group of the probe molecules, representing the acidic proton peak, respectively. The other protons corresponding to the aromatic rings appeared in the range of 6.2–8.2 ppm. Addition of fluoride ion (5.0 equiv.) to the solution of **B1** led the broadening of the N-H peak at 11.5 ppm and the signals at $\delta=5.2$ ppm corresponding to the $-\text{NH}_2$ proton experienced up-field shifts, which increases the electron density in the nitro aniline moiety favouring the ICT. Moreover, a new peak corresponding to HF_2^- appeared at 16 ppm, confirming deprotonation which eventually triggers enhancement in the electron density at the phenyl ring containing the $-\text{NH}_2$ group resulting the up-field shift of the peak at 5.2 ppm (Figure 3.7).

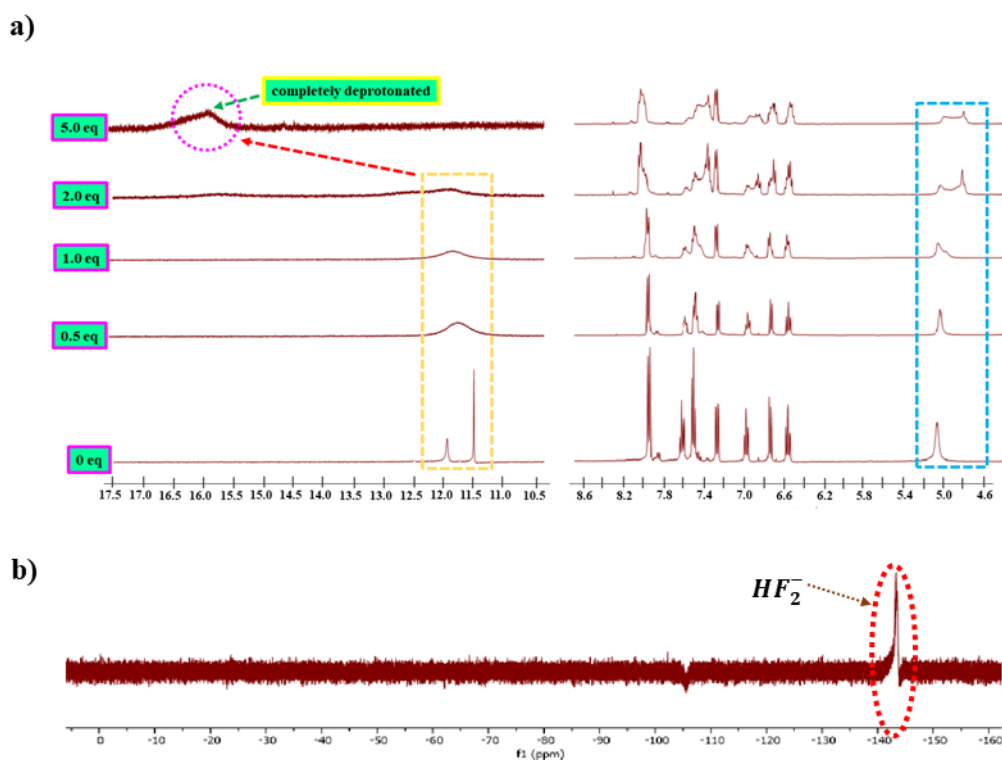


Figure 3.7: (a) Change in the ^1H NMR signals of receptor **B1** in $\text{DMSO-}d_6$ upon addition of fluoride ion; (b) ^{19}F NMR of TBAF titration to probe **B1**.

Similarly, in **B2**, signals at $\delta=8.1$ ppm undergo up-field shifts while the peak at $\delta=6.8$ ppm suffered downfield shift. Furthermore, upon the addition of 5.0 equiv. of F^- ions, signal at 11.8 ppm disappeared and a new broad singlet signal at around $\delta 16.0$ ppm was detected, corresponding to the formation of HF_2^- , providing evidence of deprotonation upon increased concentration of F^- ions (Figure 3.8). The N-H deprotonation by F^- ion enhances the electron density of the nitro substituted aniline moiety due to delocalization of the excess electron density, resulting in an up-field shift of the aromatic proton signals and eventually reinforces charge transfer in the nitroaniline moiety. Furthermore, the downfield shift of one of the aromatic CH protons of **B2** revealed the involvement of $\text{CH}\dots\text{F}^-$ interaction. The ^1H -NMR titration study concluded that both molecules interact with fluoride ions through H-bonding followed by Brønsted acid-base deprotonation equilibrium.

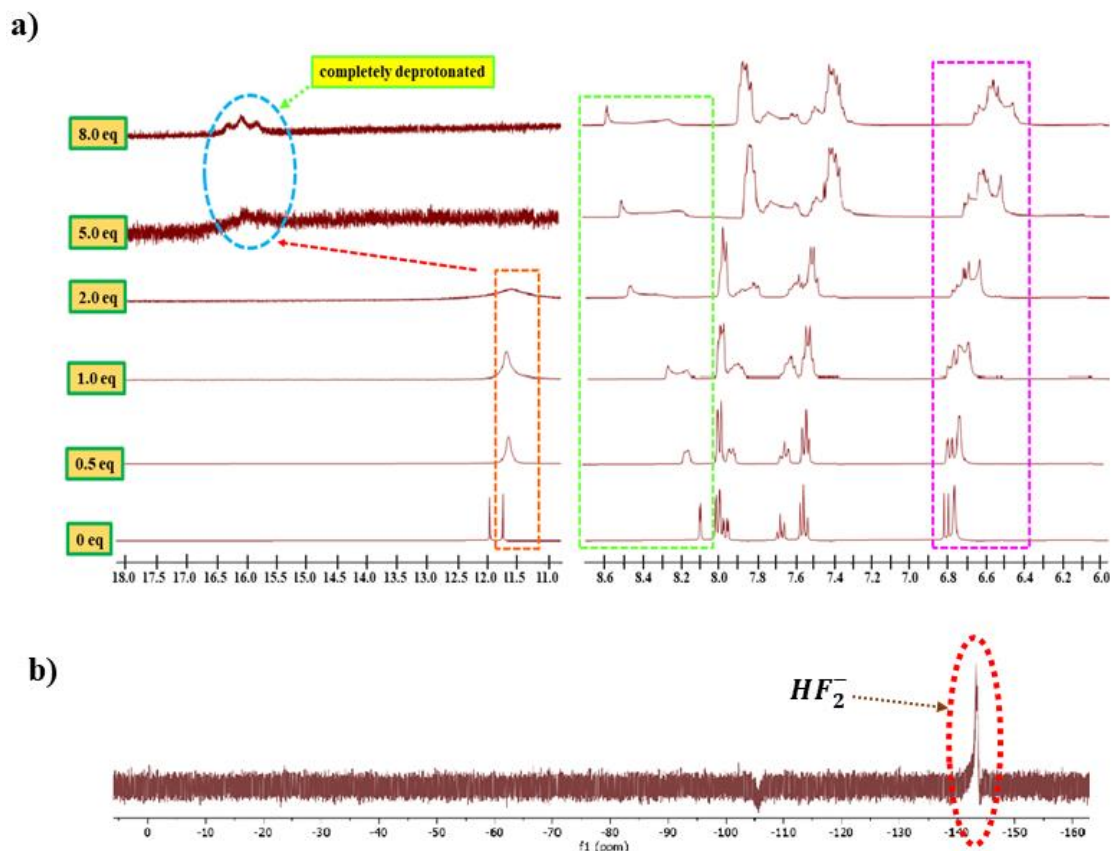


Figure 3.8: (a) Change in the $^1\text{H-NMR}$ signals of receptor **B2** in $\text{DMSO-}d_6$ upon addition of fluoride ion; (b) $^{19}\text{F NMR}$ of TBAF titration to probe **B2**.

3.3.4. Fluoride recognition study of **B1** and **B2** in aqueous medium

3.3.4.1. UV-Vis spectroscopy study

Although compounds **B1** and **B2** exhibits notable sensitivity to fluoride ions in organic media, their affinity decreases even in the presence of small amounts of water due to the unfavourable deprotonation equilibrium. To enhance the stability of the conjugate base of the probe molecules, the in-situ metal complexation strategy (hypothesis 1) was attempted. The affinity of compounds **B1** and **B2** towards various metal salts (NaCl , VCl_3 , MnCl_2 , CoCl_2 , $\text{NiCl}_2 \cdot 6\text{H}_2\text{O}$, $\text{CuCl}_2 \cdot 2\text{H}_2\text{O}$, ZnCl_2 , SrCl_2 , BaCl_2 , CaCl_2 , MgCl_2 , FeCl_2) was tested. Chloride salts of metal ions were selected because the probe molecules **B1** and **B2** showed no affinity for chloride. It was observed that both probe molecules did not exhibit affinity for any of the tested metal ions (Figure 3.9 a-b). However, the addition of an aqueous solution of Ni^{2+} ions to the $\text{B1} \cdot \text{F}^-$ solution caused a colour change to yellowish green

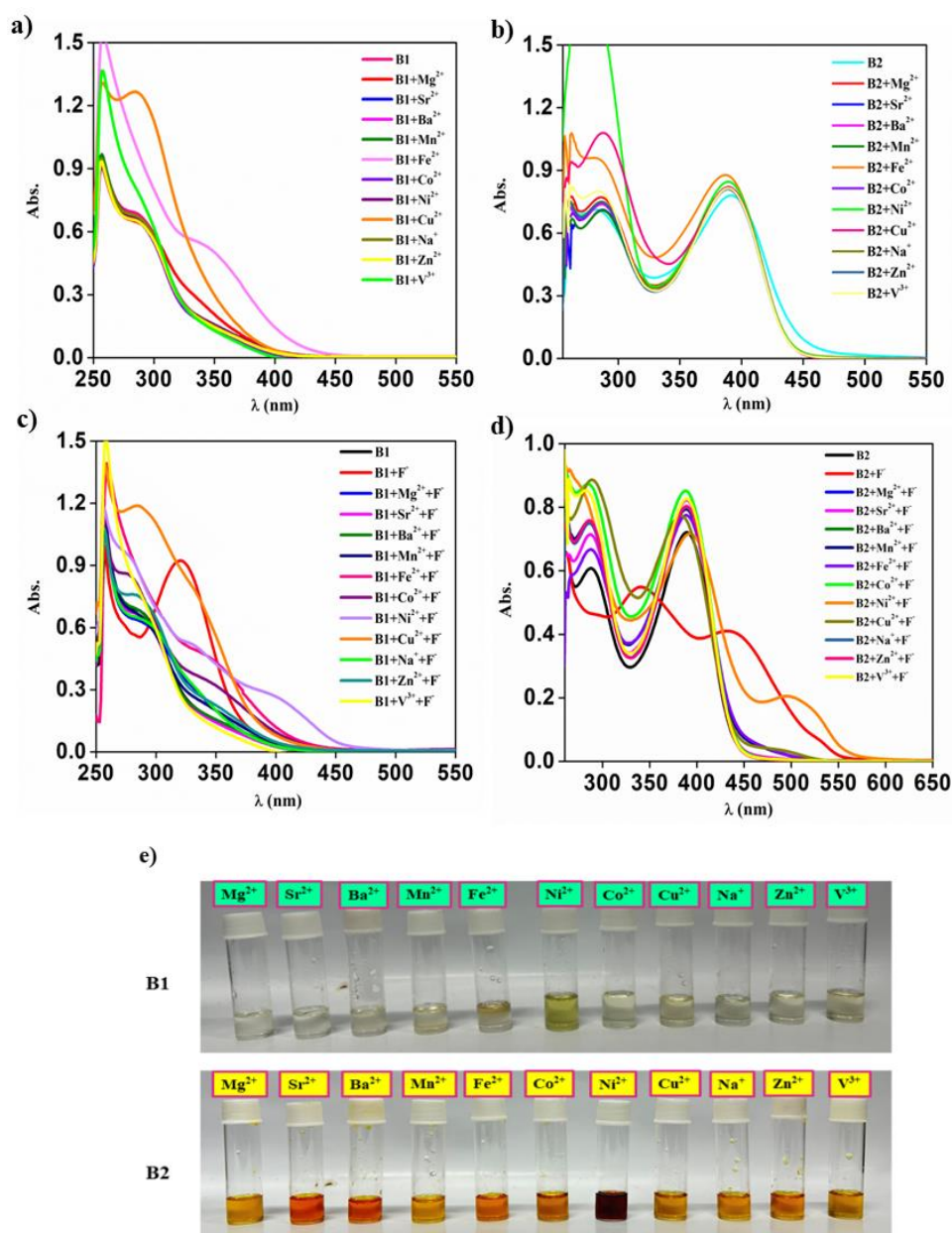


Figure 3.9: (a,c) UV-Vis absorbance of **B1** [6×10^{-5} M] in DMSO solution upon addition of different metal salts [10×10^{-3} M] (NaCl, MgSO₄, VCl₃, MnCl₂, FeSO₄, CoCl₂, NiCl₂.6H₂O, CuCl₂.2H₂O, ZnCl₂, SrCl₂, BaSO₄) as aqueous solution in absence/presence of F⁻ ion; (b,d) UV-Vis absorbance of **B2** [6×10^{-5} M] in DMSO solution upon addition of different metal salts [10×10^{-3} M] (NaCl, MgSO₄, VCl₃, MnCl₂, FeSO₄, CoCl₂, NiCl₂.6H₂O, CuCl₂.2H₂O, ZnCl₂, SrCl₂, BaSO₄) as aqueous solution in absence/presence of F⁻ ion; (e) Colorimetric changes upon the above addition.

(Figure 3.9e). The absorption spectra displayed a bathochromic shift of approximately 70 nm for the peak at 330 nm of **B1**·F⁻ solution upon addition of aqueous Ni²⁺ ions, along with the evolution of a broad peak at 400 nm (Figure 3.9c). Similarly, in the case of the **B2**·F⁻ solution, the solution's colour changed from orange to blood red upon the addition of Ni²⁺ ions in water with the emergence of a broad peak around 480 – 550 nm (Figure 3.10). The other metal ion solution led to the disappearance of the absorption peak at 400 nm, which is characteristic of the interaction between **B2** and fluoride ions. This observation indicated the stabilization of **B2** by Ni²⁺ ions, whereas other metal ions could not stabilize both **B1**⁽⁻⁾ and **B2**⁽⁻⁾, shifting the deprotonation equilibrium towards the left in aqueous medium (Figures 3.9d). Gradual addition of aqueous NaF solution to **B1** and **B2** in the presence of Ni²⁺ ions resulted in a gradual increase in the absorption peak intensity. Similar observation was not found in absence of Ni²⁺ ion. However, **B2** showed some significant change in the UV-Vis spectrum in the presence of large excess of aqueous NaF solution but the colorimetric change is not differentiable to the naked eye suggesting the inability of NaF(aq) to deprotonate the acidic protons from the probe molecules. The plot of absorbance of the peak at 350 nm of **B1** vs F⁻ ion in presence Ni(II) ion showed good linear fitting. The data of **B2** deviation from linearity at high concentration which might be due to the possibility of second deprotonation owing to the presence of the -NO₂ group. The limit of detection (LOD) value was calculated using the formula $3.3 \times SD/m$, where *SD* is the standard deviation of the blank and *m* is the slope of the calibration plot in the presence of metal ions. The calculated LOD for the probe molecule **B1** and **B2** in the presence of Ni(II) salt was found to be 0.5 ppm and 0.3 ppm, respectively (Figure 3.10). The incorporation of inbuilt charge transfer moiety in **B2** enhances the colorimetric response as well the LOD value. This study clearly indicates that thiourea probe molecules can be used for sensing fluoride ions in aqueous media in the presence of Ni²⁺ ion. The UV-Vis study in DMSO medium concluded that both the probe molecule **B1** and **B2** have affinity for AcO⁻ in DMSO medium. However, in presence of Ni²⁺(aq) solution the affinity as well as the interference of the AcO⁻ ion decreases drastically which might be due to the formation stable Ni(AcO)₂ salt before AcO⁻ starts participating in the deprotonation. This study concluded that the incorporation of Ni(II) also enhances the selectivity (Figure 3.11).

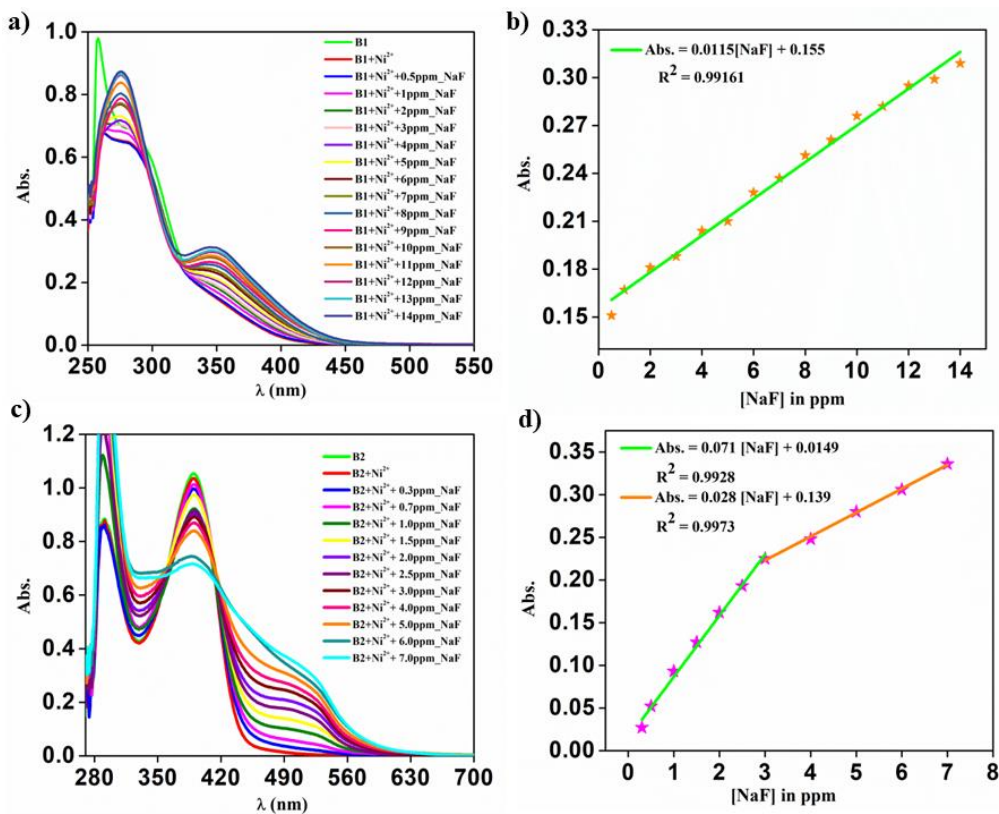


Figure 3.10: UV-Vis spectra of (a) **B1** [6×10^{-5} M] with varying NaF (in ppm) concentration in presence of Ni^{2+} cation [10×10^{-3} M]; (b) Calibration curve of the above titration; (c) **B2** [6×10^{-5} M] with varying NaF (in ppm) concentration in presence of Ni^{2+} cation [10×10^{-3} M]; (d) Calibration curve of the above titration.

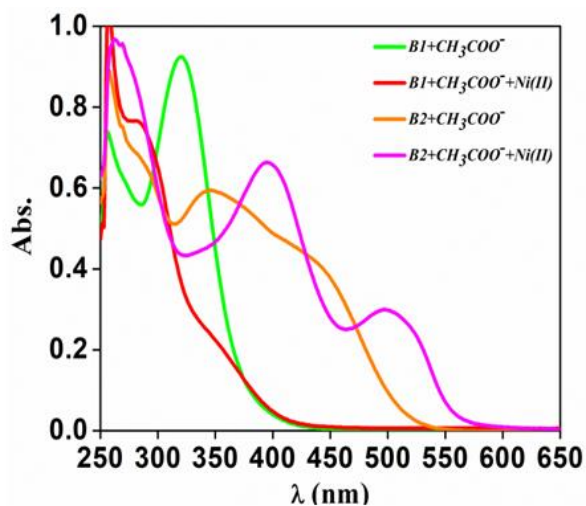


Figure 3.11: Interference study of **B1/B2** against acetate ion in absence and presence of Ni(II) ion.

3.3.4.2. Electrochemical study

To further validate our experiment, an electrochemical study was conducted. The electrochemical behaviour of **B1** and **B2** in DMSO was analysed using cyclic voltammetry and differential pulse voltammetry techniques upon the stepwise addition of NaF and NiCl₂. **B1** exhibited reduction peak at -1.02 V, while **B2** exhibited reduction peak at -1.3 V and an oxidation peak at 0.55 V. However, addition of F⁻ ions resulted in a quasi-reversible redox system with E_{pc} = -1.39 V and E_{pa} = 1.04 V for **B1**, and E_{pc} = -1.20 V and E_{pa} = 0.55 V for **B2**. Subsequently, addition of aqueous NiCl₂ to the **B1**·F⁻ solution caused the anodic peak to shift towards a less positive potential (E_{pa} = 0.03 V) and the appearance of the peaks corresponding to the Ni⁺/Ni²⁺ redox couple (Figure 3.12). Similarly, the addition of Ni(II) to the mixture of **B2** and F⁻ resulted in the anodic peak of **B2** shifting to a higher

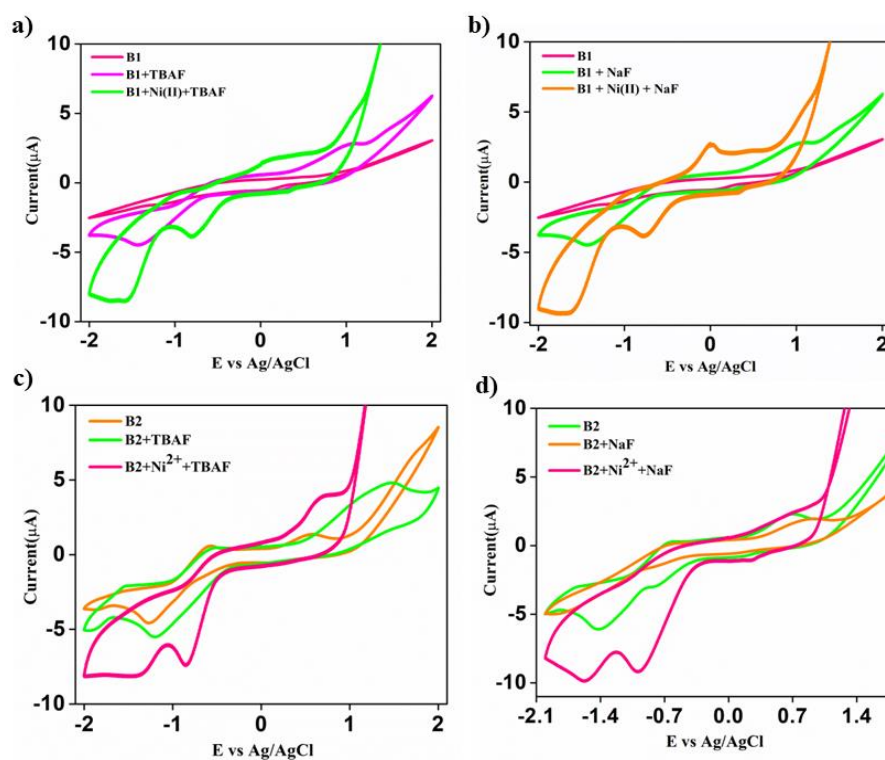


Figure 3.12: Cyclic voltammogram recorded in 0.01 M TBAP (DMSO) (a) **B1** [6×10^{-4} M] in presence of TBAF [1×10^{-3} M] presence of Ni²⁺ [1×10^{-3} M]; (b) **B1** [6×10^{-4} M] in presence of NaF [1×10^{-3} M] presence of Ni²⁺ [1×10^{-3} M]; (c) **B2** [6×10^{-4} M] in presence of TBAF [1×10^{-3} M] presence of Ni²⁺ [1×10^{-3} M]; (d) **B2** [6×10^{-4} M] in presence of NaF [1×10^{-3} M] presence of Ni²⁺ [1×10^{-3} M].

potential ($E_{pa} = 0.69$ V) and the appearance of two reduction peaks at $E_{pc} = -0.85$ V and $E_{pc} = -1.35$ V, corresponding to the formation of Ni^{2+}/Ni^+ and some part getting converted to Ni^{3+}/Ni^+ , respectively [25,26]. This observation pointed to the in-situ complexation of the deprotonated probe molecule with the Ni(II) ion. To investigate the kinetics of the electrochemical behaviour on a glassy carbon electrode (GCE), the effect of scan rate on electrochemical signals was recorded for samples containing all three components (**B1** or **B2**, F^- , and $NiCl_2$) at scan rates of 50, 60, 70, 80, 90, and 100 $mV \cdot s^{-1}$. It was observed that the anodic peak shifted slightly to a more positive potential, and the current increased linearly with increasing scan rate. The corresponding Randles-Sevcik plot, *i.e.* the plot of peak current (I_p) vs. the square root of scan rate ($v^{1/2}$), linearity with significant intercept revealing the diffusion-cum-adsorption controlled kinetic processes for all three systems (Figure 3.13) [27,28].

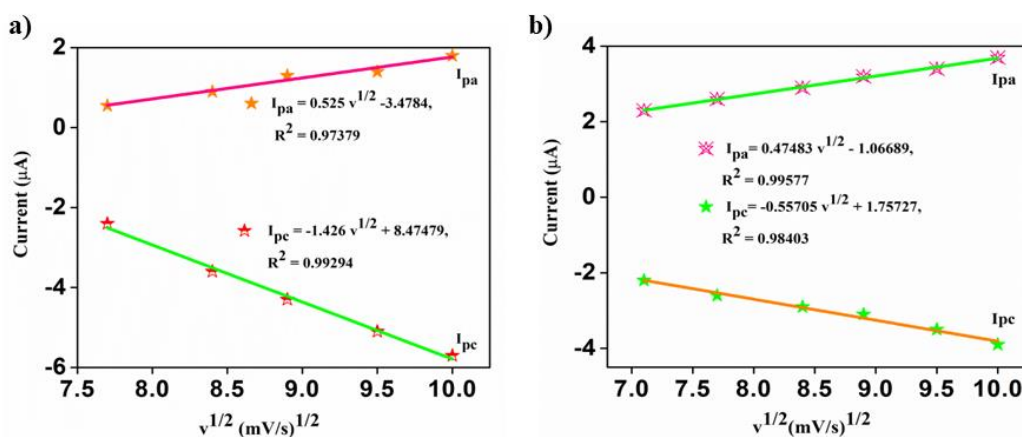


Figure 3.13: (a) RS plot for **B1.F⁻** in presence Ni^{2+} ion; (b) RS plot for **B2.F⁻** in presence Ni^{2+} ion.

Differential pulse voltammetry (DPV) of **B1** and **B2** solutions in DMSO in presence of Ni^{2+} (aq), upon gradual addition of $NaF(aq)$, was monitored by sweeping the potential from 0 to -2 V. For the DPV experiment, the reduction peaks of the deprotonated probe molecules were considered. In both cases, the peak potential shifted to a lower potential and a linear decrease in the current of the cathodic peak with increasing concentration of fluoride of F^- . The change in peak height against the concentration of F^- showed good linear fitting in both cases with appreciable RMSD values (figure 3.14) [29,30]. The DPV experiment suggested that probe molecules **B1** and **B2** could be used as electrochemical sensor probes for detecting F^- ions in water medium in presence of Ni^{2+} . The LOD value calculated for

the detection of aqueous F^- ions are 0.7 ppm for **B1**, whereas **B2** has an LOD value of 0.4 ppm in the presence of Ni^{2+} ion (Figure 3.14).

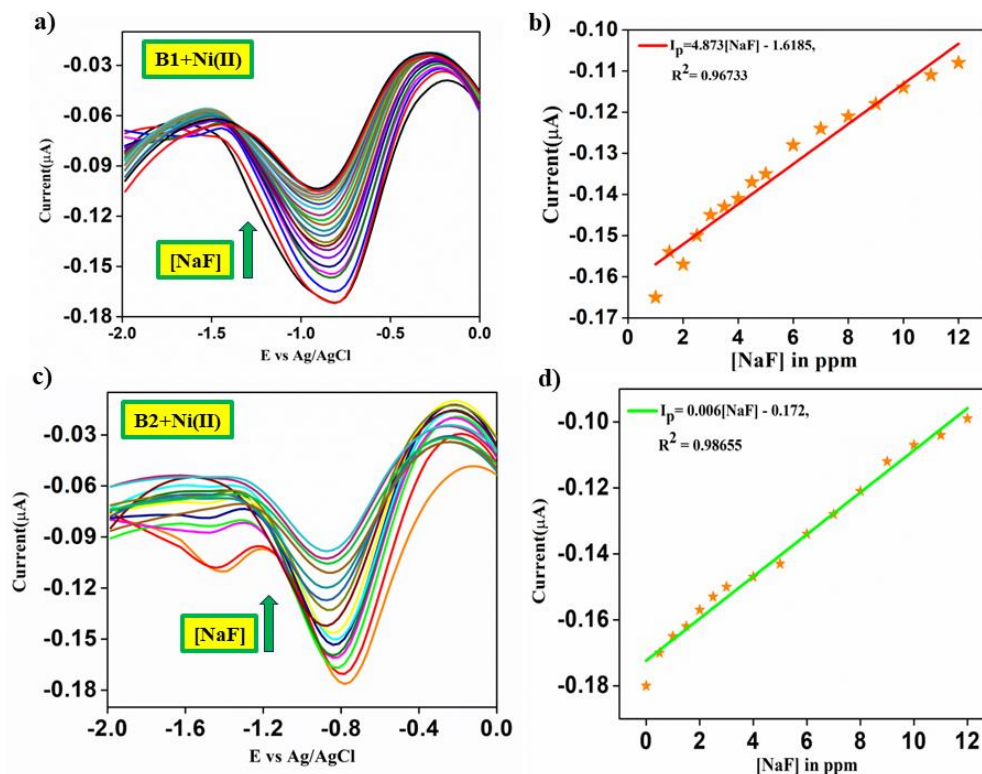


Figure 3.14: (a) Change in the DPV plots of **B1** [$6 \times 10^{-4}M$ in DMSO] upon gradual addition of NaF(aq) in presence of Ni (II) salt [$1 \times 10^{-3}M$ in water]; (b) The calibration curve for the titration shown in (a); (c) Change in the DPV plots of **B2** [$6 \times 10^{-4}M$ in DMSO] upon gradual addition of NaF(aq) in presence of Ni (II) salt [$1 \times 10^{-3}M$ in water]; (d) the calibration curve for the titration shown in (c).

3.3.5. Investigation of the sensing mechanism

To understand the role of $Ni(II)$ ion in improving the sensing efficiency of probe **B1** and **B2** the in-situ formed complex was precipitated and characterised with FTIR spectroscopy. The peaks at 511 cm^{-1} and 678 cm^{-1} corresponding to O-Ni-N rocking and Ni-N stretching vibration inferred the complexation of the deprotonated probe molecule with $Ni(II)$ ion. (Figure 3.15) [31].

To decipher the oxidation state of the metal ion, EPR analysis of the reaction mixture was performed in frozen aqueous DMSO solution. The X-band (9.44 GHz) EPR spectra of **B1** and **B2**, upon stepwise addition of $NiCl_2$ (aq) and $F^-(aq)$ did not show any peak, confirming the diamagnetic nature of the $Ni(II)$ complexation (Figure 3.16).

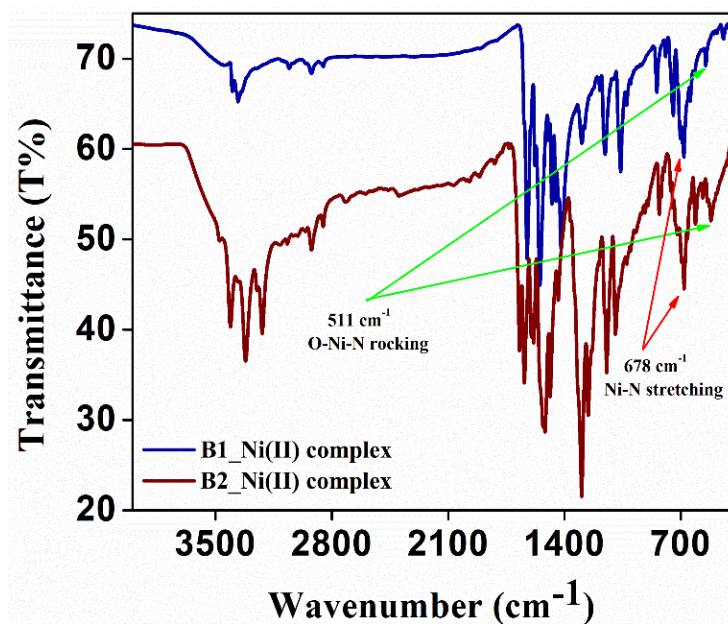


Figure 3.15: FTIR spectra of isolated Ni(II) complex of **B1** and **B2**.

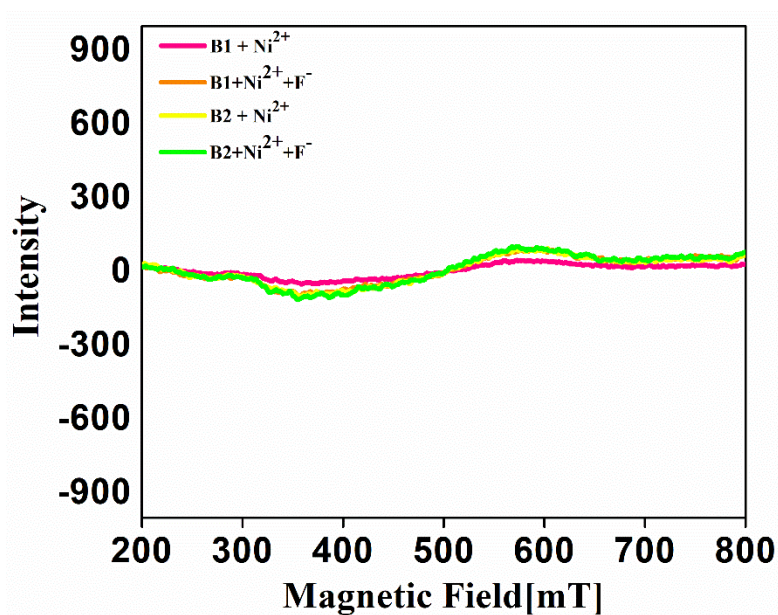


Figure 3.16: EPR spectra (Freq:9441.38 MHz, 100 K, DMSO): Pink: addition of NiCl₂ (aq.) to the **B1** solution; Orange: addition of NiCl₂(aq) to the **B1** solution followed by F⁻ in DMSO; Yellow: addition of NiCl₂ (aq.) to the **B2** solution; Green: addition of NiCl₂(aq) to the **B2** solution.

3.3.6. Validation of the method with real life sample

Finally, the methodology was validated by quantifying the fluoride ion concentration in real water samples collected from Dokmoka village in the Karbi Anglong district of Assam, India. For the analysis, a 3 mL aliquot of 6×10^{-5} M solution of **B1** and **B2** was placed in a cuvette, respectively, to which 50 μ L of 10×10^{-3} M NiCl₂ solution in aqueous medium was added. Subsequently, 50 μ L of the water sample was introduced to the mixture. The

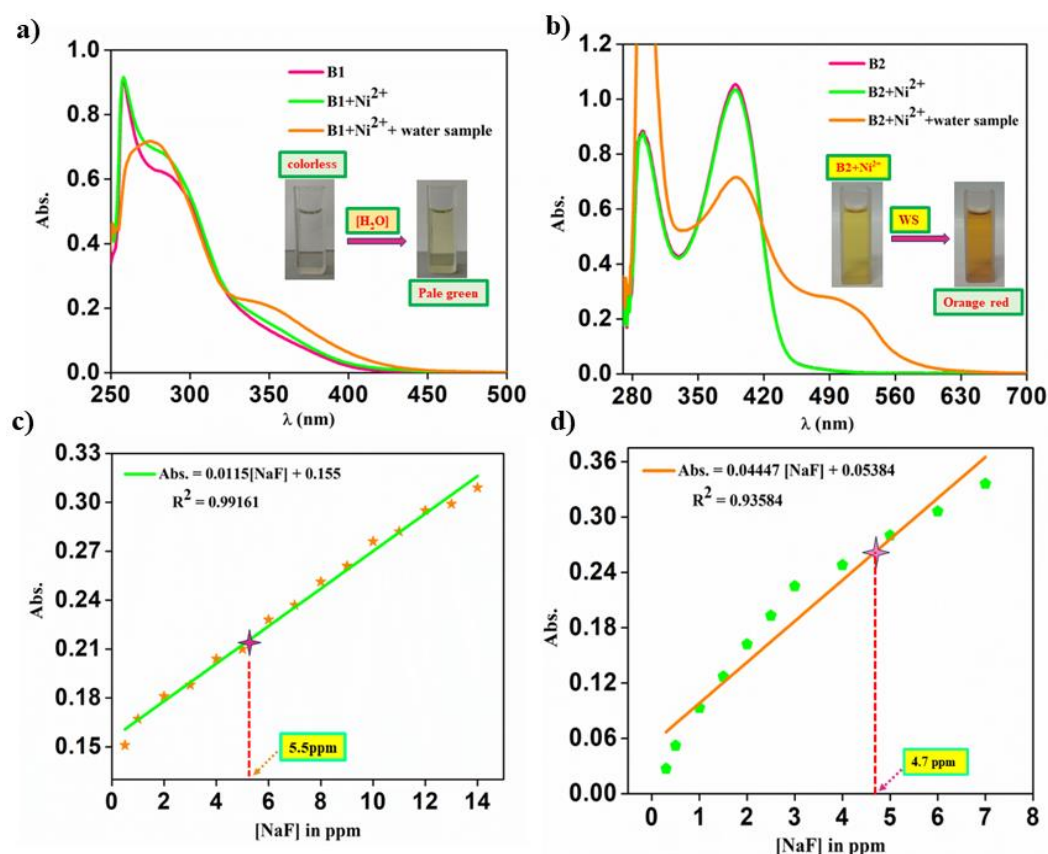


Figure 3.17: (a) Change in the UV-Vis spectra of **B1** upon addition of 50 μ L of water sample in presence of Ni(II) ion; (b) Change in the UV-Vis spectra of **B1** upon addition of 50 μ L of water sample in presence of Ni(II) ion; (c) Corresponding calibration plot; the pink mark indicates the absorbance of the unknown water sample with **B1**; (d) Corresponding calibration plot; the pink mark indicates the absorbance of the unknown water sample with **B2**.

resultant colorimetric response was analysed using a UV-Vis spectrometer, and the absorbance at wavelengths of 360 nm and 500 nm was measured (Figure 3.17). The absorbance data of the calibration plot showed good linear fitting for **B1** and **B2** (Figure 3.10c,d). As observed earlier **B2** showed deviation at higher concentration (above 4 ppm). The absorbance data obtained were then compared with the previously established calibration plot to determine the fluoride ion concentration in the water sample. The analysis revealed a fluoride ion concentration of 5.5 ppm with **B1** and 4.7 ppm with **B2** in the water collected from Dokmoka village. This result was further corroborated by measurements using a fluoride ion-selective electrode (5.0 ppm), thereby confirming the accuracy and reliability of our methodology.

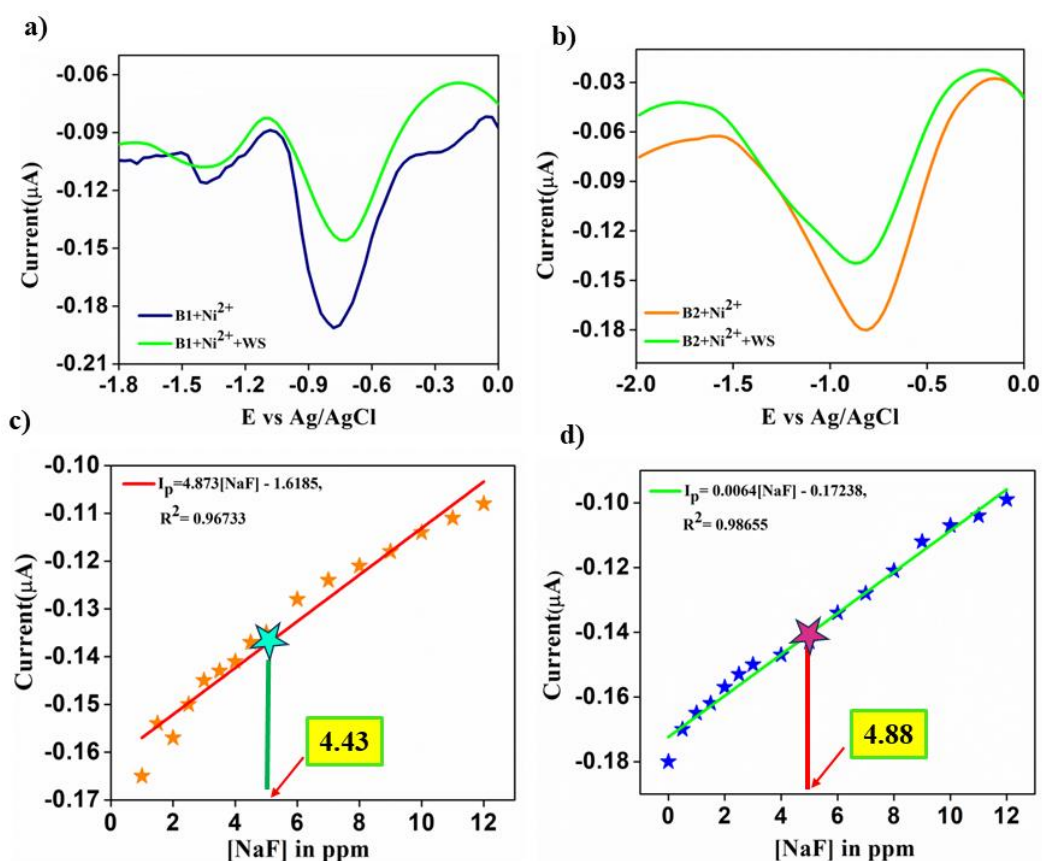


Figure 3.18: (a) DPV of **B1** upon addition of 100 μL of water sample in presence of $\text{Ni}(\text{II})$ ion; (b) DPV of **B2** upon addition of 100 μL of water sample in presence of $\text{Ni}(\text{II})$ ion; (c) Corresponding calibration plot; the green mark indicates the concentration of the unknown water sample with **B1**; (d) Corresponding calibration plot; the pink mark indicates the concentration of the unknown water sample with **B2**.

Similarly, we performed differential pulse voltammetry (DPV) measurement for the detection of fluoride content in the same water sample. Here, 200 μL of Ni(II) (10×10^{-3} M) was added to 30 mL of **B1** and **B2** solution (1×10^{-3} M), followed by the addition of 100 μL of the water sample having known concentration of fluoride and the calibration curve was obtained. The DPV of the water sample collected was measured in the same condition. The DPV showed the concentration of fluoride to be 4.4 ppm with **B1** and 4.8 ppm with **B2** in the presence of Ni(II) ions. The results obtained are consistent with the concentrations revealed by the ion-selective electrode (Figure 3.18).

3.4. Conclusion

Both probe **B1** (*N*-((2-aminophenyl)carbamothioyl)benzamide) and probe **B2** (*N*-((2-amino-4-nitrophenyl)carbamothioyl)benzamide) can colorimetrically and electrochemically sense fluoride ions in a DMSO medium, with probe **B2** exhibiting a higher affinity for fluoride ions compared to probe **B1**. The methodology for sensing aqueous fluoride ions using **B1** and **B2** has been validated through UV-Vis spectroscopy and electrochemical methods. The incorporation of a nitro group ($-\text{NO}_2$) enhances the sensitivity of the probes but decreases their selectivity in DMSO medium. Both **B1** and **B2** can detect fluoride ion in aqueous medium upon use of Ni(II) ion in the sensing medium. The limit of detection (LOD) values are 0.5 ppm for **B1** and 0.3 ppm for **B2** using the UV-Vis method, and 0.7 ppm for **B1** and 0.4 ppm for **B2** using the differential pulse voltammetry (DPV) method. Incorporation of Ni(II) ions in sensing methodology is also found to improve the fluoride selectivity by nullifying the interference from acetate ion. This sensing methodology has been successfully applied to real-life samples, demonstrating the effective detection of fluoride in groundwater.

3.5. References:

- [1] Li, L. The biochemistry and physiology of metallic fluoride: action, mechanism, and implications. *Critical Reviews in Oral Biology & Medicine*, 14(2):100-114, 2003.
- [2] Buzalaf, M. A. R., Pessan, J. P., Honório, H. M., and Ten Cate, J. M. Mechanisms of action of fluoride for caries control. *Fluoride and the oral environment*, 22:97-114, 2011.
- [3] Buzalaf, M. A. R. *Fluoride and the oral environment* (Vol. 22). Karger Medical and Scientific Publishers, Vol.22, 2011.

- [4] Jose, D. A., Kumar, D. K., Ganguly, B., and Das, A. Efficient and simple colorimetric fluoride ion sensor based on receptors having urea and thiourea binding sites. *Organic letters*, 6(20):3445-3448, 2004.
- [5] Okudan, A., Erdemir, S., and Kocyigit, O. 'Naked-eye' detection of fluoride and acetate anions by using simple and efficient urea and thiourea based colorimetric sensors. *Journal of molecular structure*, 1048:392-398, 2013.
- [6] Tarai, A., and Baruah, J. B. Conformation and visual distinction between urea and thiourea derivatives by an acetate ion and a hexafluorosilicate cocrystal of the urea derivative in the detection of water in dimethylsulfoxide. *ACS omega*, 2(10):6991-7001, 2017.
- [7] Effendhy, N. D., Roto, R., and Siswanta, D. Advancing fluoride (F⁻) detection: Exploring the potential of digital color analysis with a novel thiourea receptor. *Microchemical Journal*, 197:109819, 2024.
- [8] Cao, X., Zhao, N., Lv, H., Gao, A., Shi, A., and Wu, Y. 4-Nitrobenzene thiourea self-assembly system and its transformation upon addition of Hg²⁺ ion: Applications as sensor to fluoride ion. *Sensors and Actuators B: Chemical*, 266, 637-644, 2018.
- [9] Razak, N. H. A., Tan, L. L., Hasbullah, S. A., and Heng, L. Y. Reflectance chemosensor based on bis-thiourea derivative as ionophore for copper (II) ion detection. *Microchemical Journal*, 153:104460, 2020.
- [10] Oyeka, E. E., Asegbeloyin, J. N., Babahan, I., Eboma, B., Okpareke, O., Lane, J., and Izuogu, D. C. Synthesis, crystal structure, computational analysis and biological properties of 1-(4-chlorobenzoyl)-3-[2-(2-{2-[3-(4-chlorobenzoyl)-thioureido]-ethoxy} ethoxy) ethyl]-thiourea and its Ni (II) and Cu (II) complexes. *Journal of Molecular Structure*, 1168:153-164, 2018.
- [11] Kafi-Ahmadi, L., and Shirmohammadzadeh, L. Synthesis of Co(II) and Cr(III) salicylidenic Schiff base complexes derived from thiourea as precursors for nano-sized Co₃_33O₄_44 and Cr₂_22O₃_33 and their catalytic, antibacterial properties. *J Nanostruct Chem*, 7(2):179–190. 2017.
- [12] Nishat, N., Ahmad, S., and Rahisuddin, T. A. Synthesis and Characterization of Antibacterial Polychelates of Urea–Formaldehyde Resin with Cr(III), Mn(II), Fe(III),

- Co(II), Ni(II), Cu(II), and Zn(II) Metal Ions. *J. Appl. Polym. Sci.*, 100(2), 928–936, 2006.
- [13] Fayomi, O. M., ShaAto, R., Wuana, R. A., Igoli, J. O., Moodley, V., and Van Zyl, W. E. Synthesis, Characterization and Antibacterial Studies of Some Metal Complexes of N-DI (Pyridin-2-Yl) Thiourea Derivatives. *Int. Res. J. Pure Appl. Chem.*, 16(3), 1–31, 2018.
- [14] Amendola, V., Boiocchi, M., Fabbrizzi, L., and Palchetti, A. Anion Receptors Containing-NH Binding Sites: Hydrogen-Bond Formation or Neat Proton Transfer? *Chemistry–A European Journal*, 11(1): 120-127, 2005.
- [15] Boiocchi, M., Del Boca, L., Esteban-Gómez, D., Fabbrizzi, L., Licchelli, M., and Monzani, E. Anion-induced urea deprotonation. *Chemistry–A European Journal*, 11(10):3097-3104, 2005.
- [16] Li, D. Benzimidazole-isoquinolinone functioned thiourea for selective and reversible recognition of fluoride ion. *Journal of Molecular Structure*, 1206:127631, 2020.
- [17] Carreira-Barral, I., Rodriguez-Blas, T., Platas-Iglesias, C., de Blas, A., and Esteban-Gomez, D. Cooperative anion recognition in copper (II) and zinc (II) complexes with a ditopic tripodal ligand containing a urea group. *Inorganic Chemistry*, 53(5):2554-2568, 2014.
- [18] Das, R., Talukdar, D., Sarma, P. J., Kuilya, H., Thakuria, R., Choudhury, D., and Mahanta, S. P. Colorimetric detection of fluoride ions in aqueous medium using thiourea derivatives: a transition metal ion assisted approach. *Dalton Transactions*, 50(42):15287-15295, 2021.
- [19] Shao, J., Lin, H., and Lin, H. K. A simple and efficient colorimetric anion sensor based on a thiourea group in DMSO and DMSO–water and its real-life application. *Talanta*, 75(4):1015-1020, 2008.
- [20] Devaraj, S., Saravanakumar, D., and Kandaswamy, M. Dual responsive chemosensors for anion and cation: Synthesis and studies of selective chemosensor for F⁻ and Cu (II) ions. *Sensors and Actuators B: Chemical*, 136(1):13-19, 2009.
- [21] Wu, F. Y., Hu, M. H., Wu, Y. M., Tan, X. F., Zhao, Y. Q., and Ji, Z. J. Fluoride-selective colorimetric sensor based on thiourea binding site and anthraquinone

- reporter. *Spectrochimica Acta Part A: Molecular and Biomolecular Spectroscopy*, 65(3-4):633-637, 2006.
- [22] Kumar, V., Kaushik, M. P., Srivastava, A. K., Pratap, A., Thiruvengatam, V., and Row, T. G. Thiourea based novel chromogenic sensor for selective detection of fluoride and cyanide anions in organic and aqueous media. *Analytica chimica acta*, 663(1):77-84, 2010.
- [23] Duke, R. M., and Gunnlaugsson, T. Selective fluorescent PET sensing of fluoride (F⁻) using naphthalimide–thiourea and–urea conjugates. *Tetrahedron Letters*, 48(45):8043-8047, 2007.
- [24] Veale, E. B., and Gunnlaugsson, T. Bidirectional photoinduced electron-transfer quenching is observed in 4-amino-1, 8-naphthalimide-based fluorescent anion sensors. *The Journal of Organic Chemistry*, 73(20):8073-8076, 2008.
- [25] Deveci, P. Synthesis, spectroscopic and cyclic voltammetry studies of novel azacrown ether containing vic-dioxime ligand and its Ni (II), Cu (II), Co (II), Cd (II) and Zn (II) complexes. *Journal of Inclusion Phenomena and Macrocyclic Chemistry*, 77:319-325, 2013.
- [26] Shiekh, R. A., Ab Rahman, I., Malik, M. A., and Luddin, N. Synthesis, spectral, electrochemical and biological studies of nitrogen donor macrocyclic ligand and its transition metal complexes. *International Journal of Electrochemical Science*, 7(12), 12829-12845, 2012.
- [27] Chu, T., Popov, I. A., Andrade, G. A., Maurya, S., Yang, P., Batista, E. R., and Davis, B. L. Linked picolinamide nickel complexes as redox carriers for nonaqueous flow batteries. *ChemSusChem*, 12(7):1304-1309, 2019.
- [28] Vaughn, B. A., Brown, A. M., Ahn, S. H., Robinson, J. R., and Boros, E. Is less more? Influence of the coordination geometry of Copper (II) picolinate chelate complexes on metabolic stability. *Inorganic chemistry*, 59(22), 16095-16108, 2020.
- [29] Donat, J. R., and Bruland, K. W. Direct determination of dissolved cobalt and nickel in seawater by differential pulse cathodic stripping voltammetry preceded by adsorptive collection of cyclohexane-1, 2-dione dioxime complexes. *Analytical chemistry*, 60(3), 240-244, 1988.

- [30] Amini, M. K., and Kabiri, M. Determination of trace amounts of nickel by differential pulse adsorptive cathodic stripping voltammetry using calconcarboxylic acid as a chelating agent. *Journal of the Iranian Chemical Society*, 2, 32-39, 2005.
- [31] Nakamoto, K. Applications in coordination, organometallic, and bioinorganic chemistry. 1997.
- [32] Hanse, A., Chabukdhara, M., Gohain Baruah, S., Boruah, H., and Gupta, S. K. Fluoride contamination in groundwater and associated health risks in Karbi Anglong District, Assam, Northeast India. *Environmental monitoring and assessment*, 191(12):782, 2019.